Supporting Information

Metallophthalocyanine-based Molecular Dipole Layer as a Universal and Versatile Approach to Realize Efficient and Stable Perovskite Solar Cells

Fangchao Li,[†] Jianyu Yuan,[†,] Xufeng Ling,[†] Lizhen Huang,[†] Nopporn Rujisamphan,[‡] Youyong Li,[†] Lifeng Chi,[†] Wanli Ma[†,*]*

[†]Institute of Functional Nano & Soft Materials (FUNSOM), Jiangsu Key Laboratory for Carbon-Based Functional Materials & Devices, Soochow University, 199 Ren-Ai Road, Suzhou Industrial Park, Suzhou, Jiangsu 215123, P. R. China

[‡]King Mongkut's University of Technology Thonburi (KMUTT) 126 Pracha Uthit Rd., Bang Mod, Thung Khru, Bangkok 10140, Thailand

Corresponding Author: jyyuan@suda.edu.cn (J. Y.); wlma@suda.edu.cn(W. Ma).

1. Grazing-incidence wide angle X-ray scattering:

GIWAXS measurements were performed at the Shanghai Synchrotron Radiation Facility (SSRF) Laboratory on Beamline BL14B1 using X-ray with a wavelength of λ=~1.24 Å. 2D GIWAXS patterns were acquired by a MarCCD mounted vertically at a distance ~194 mm from the sample with a grazing incidence angle of 0.4°and an exposure time of 50 s. The 2D GIWAXS patterns were analyzed using the FIT2D software and displayed in scattering vector q coordinates with $q = 4\pi\sin\theta/\lambda$, where θ is half of the diffraction angle and λ is the wavelength of incident X-ray.

2. Photoluminescence lifetime imaging

Figure S9 shows the schematic of the time-resolved confocal imaging system, implemented on an ISS Q2 laser scanning nanoscope (ISS Inc., Champaign, Illinois, USA). It is coupled to a Nikon TiU microscope equipped with a Nikon 60X/1.2NA water objective lens. A 405-nm pulsed diode laser was used as the excitation source.

The laser repetition rate was set to be 10 MHz for measuring the Perovskite photoluminescence lifetimes. The emission light after a 480-nm long-pass filter was collected by a single photon counting module avalanche photodiode by Excelitas (model: SPCM-AQRH-14). For each Perovskite sample, a field of 40μm x 40μm was scanned using Galvo mirrors at the sampling rate of 256 x 256 pixels. Both the laser and the scanner were synchronized to the data acquisition unit of FastFLIM by ISS, to record the time-resolved data at each pixel of the image. The phase histogram can be converted to the decay histogram for the time-domain (TD) lifetime fitting data analysis, or processed by the digital Fourier transform (DFT) for the digital frequency-domain (DFD) lifetime fitting data analysis. In TD, the lifetimes are estimated from fitting the decay profiles upon a pre-defined exponential model. In DFD, the phase delays (ϕ) and modulation ratios (m) of the emission relative to the excitation at multiple frequencies are simultaneously obtained by the DFT of the phase histogram, and then fitted upon a pre-defined exponential model to estimate the lifetimes.

3. Kelvin probe force microscopy measurements

The work function of the neat perovskite film and the films w/wo additives are characterized by KPFM through probing the surface potential difference (SPD) between Ti/Ir-coated tip and the samples. The SPD is defined as the following Eq. (1)

$$e \times SPD = WF_t + WF_s \quad (1)$$

Where e is elementary charge of electron, WF_t is the work function of Ti/Ir-coated tip, and WFs is the work function of sample surface. WF_t is calibrated using highly

ordered pyrolytic graphite (HOPG) with a constant work function of 4.60 eV. Finally, the work function of samples can be calculated by the Eq. (2):

$$WF_s = 4.60 + e(SPD_{HOPG} - SPD_s) \quad (2)$$

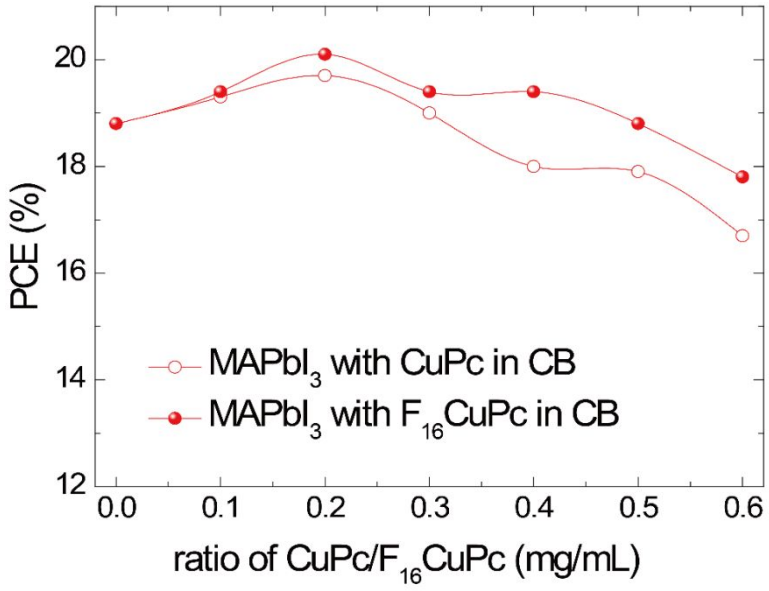

Figure S1. PCE of $MAPbI_3$ perovskite solar cells with $CuPc/F_{16}CuPc$ addition at different concentration.

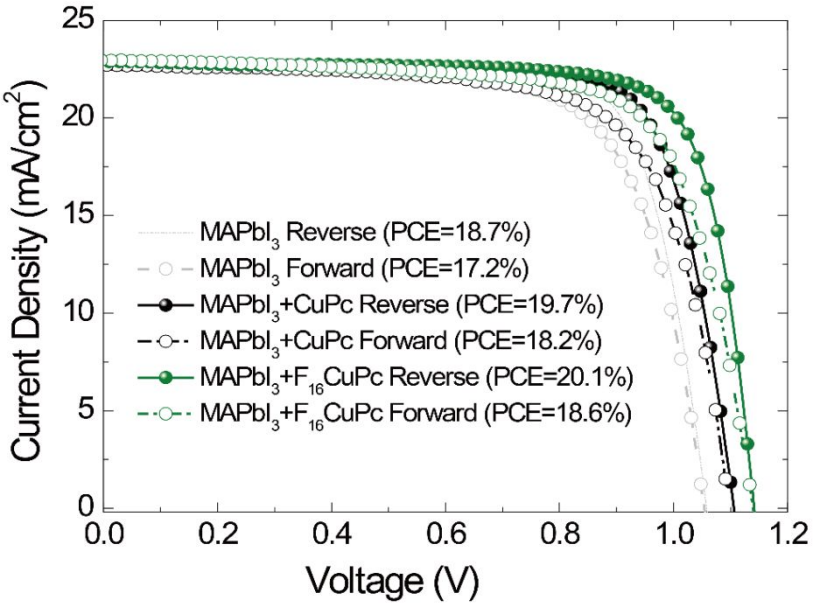

Figure S2. Current–voltage (*J-V*) curves of optimized perovskite solar cells under reverse and forward scans with/without (w/wo) CuPc or F_{16}CuPc, measured under AM 1.5 (Hysteresis index, 0.080 for $MAPbI_3$, 0.076 for $MAPbI_3$+CuPc and 0.075 for $MAPbI_3$+F_{16}CuPc).

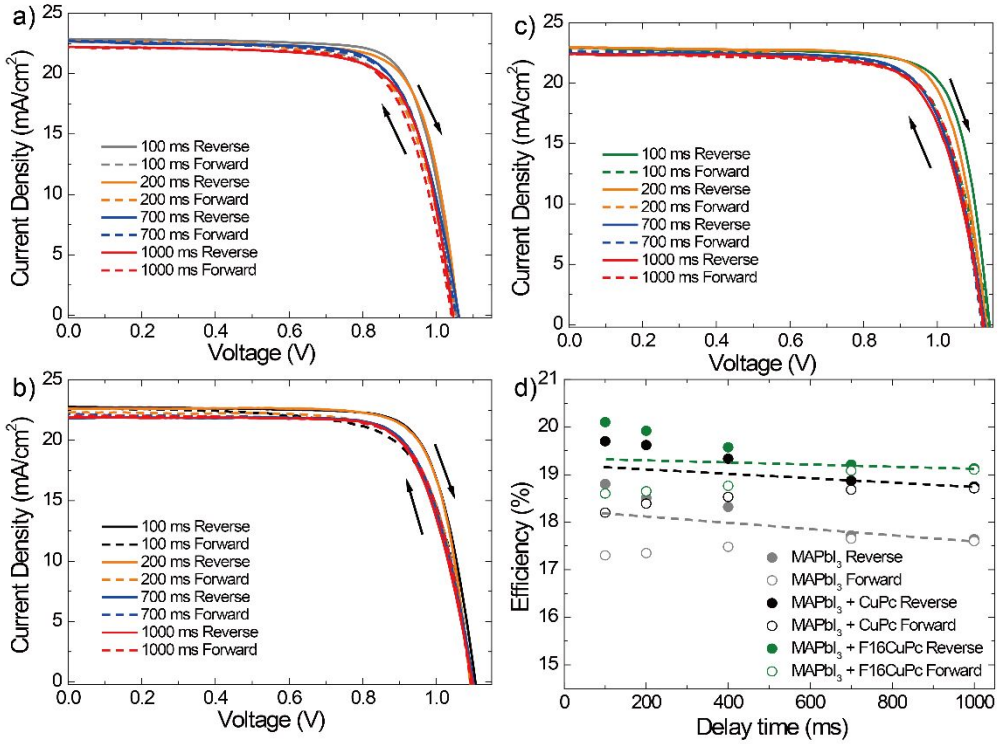

Figure S3. a-c) The hysteresis in current–voltage curves of devices w/wo additives. Arrows denote the sweep direction. d) Efficiency of devices scaning with different delay time.

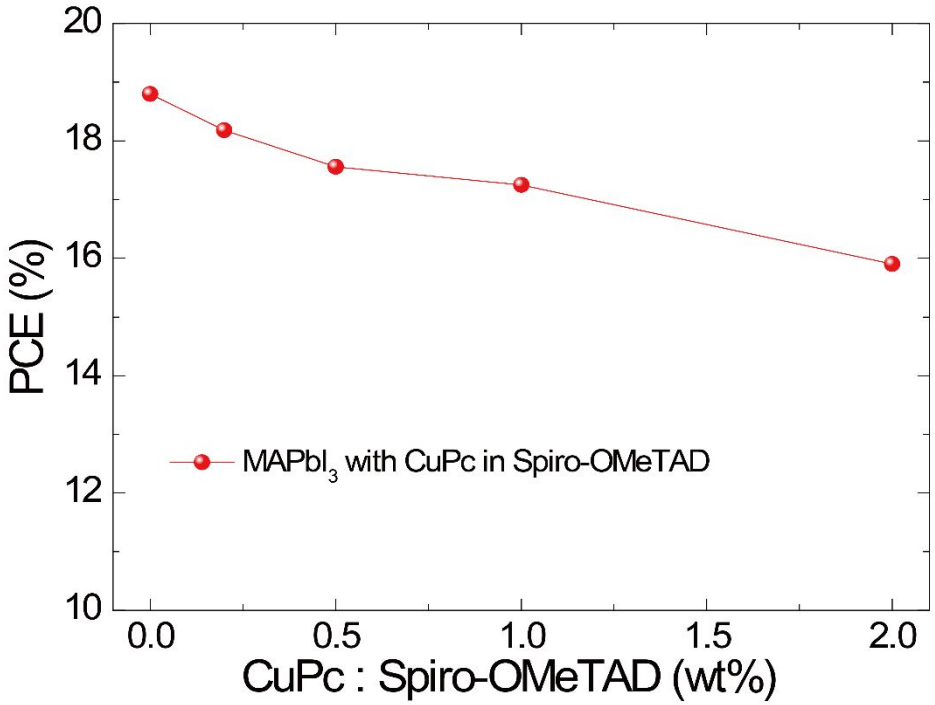

Figure S4 PCE of $MAPbI_3$ perovskite solar cells with CuPc addition into HTL Spiro-OMeTAD at different concentration.

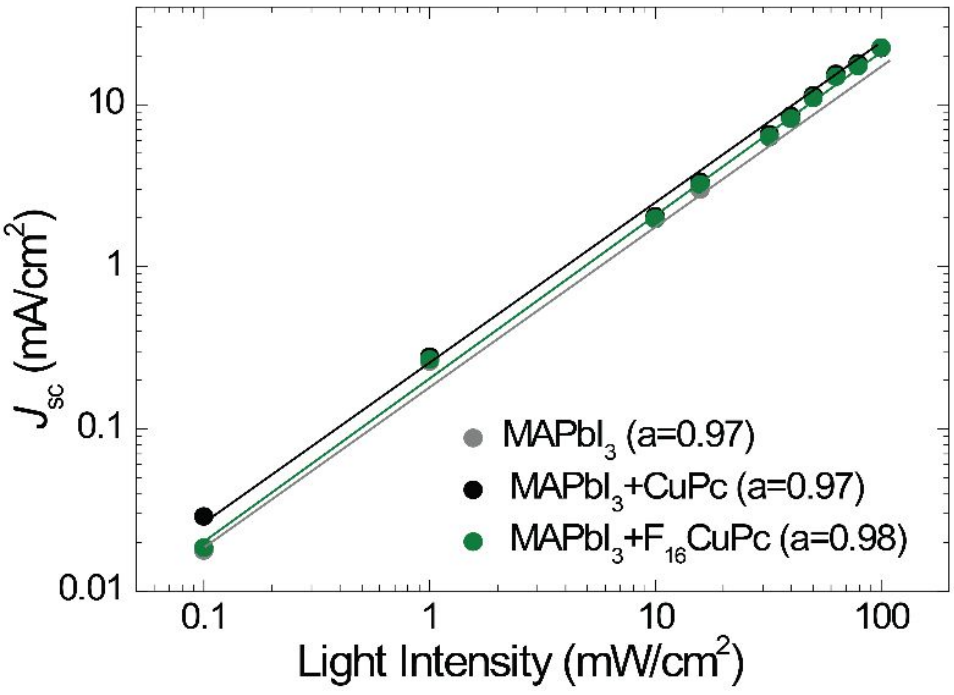

Figure S5. J_{sc} dependence on illumination intensity w/wo metallophthalocyanine additives, together with linear fits in lines.

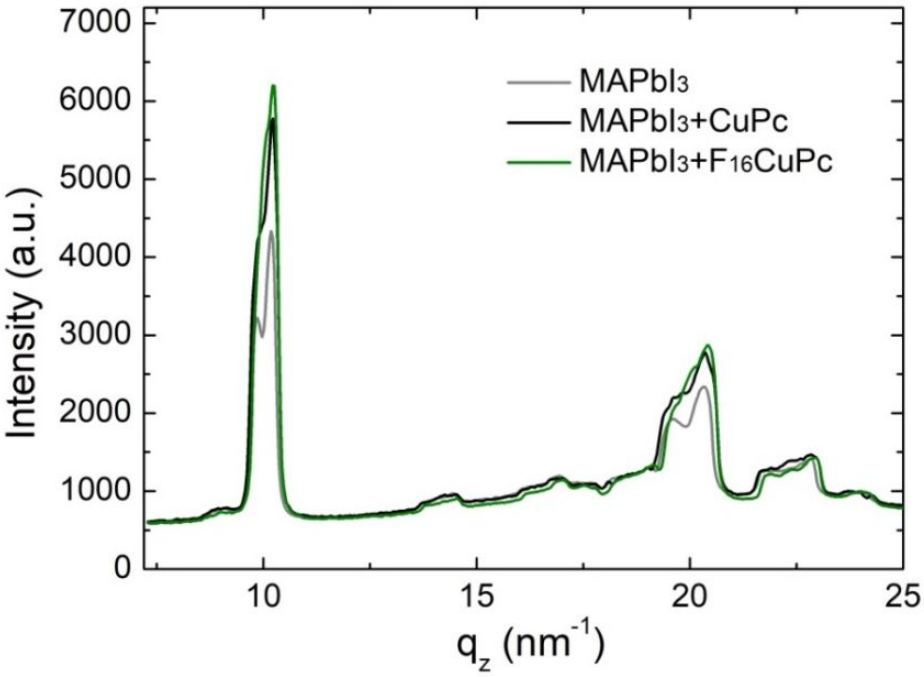

Figure S6. The out-of-plane line-cuts of (110) diffraction of perovskite films w/wo additives.

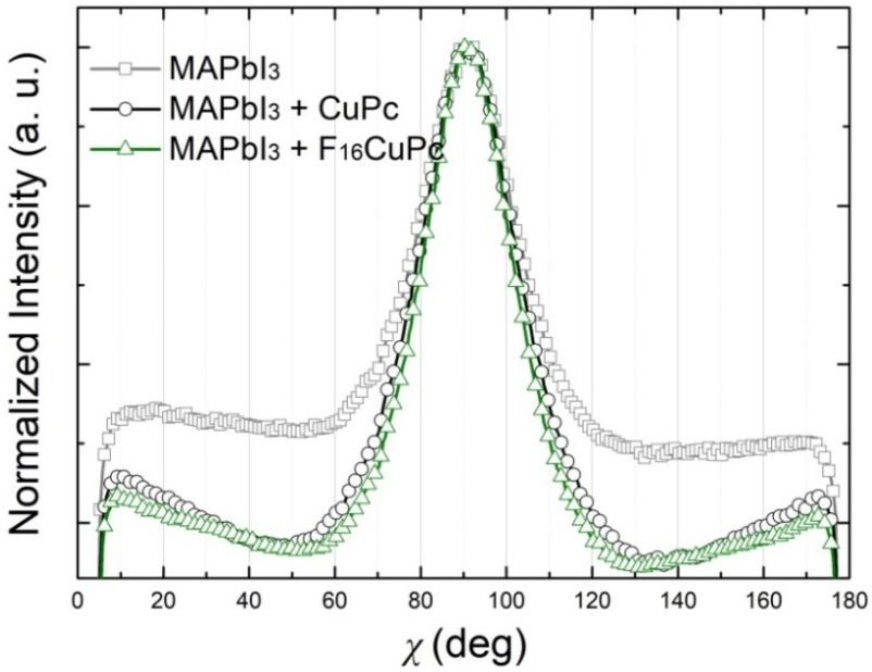

Figure S7. The pole figures extracted from the (110) for corresponding films w/wo additives.

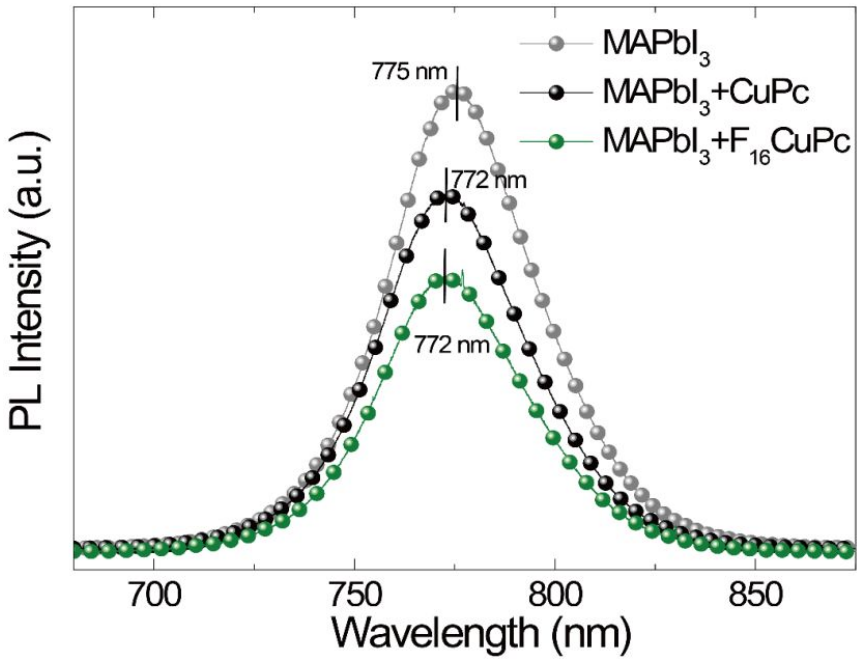

Figure S8. Steady-state PL spectra of corresponding films on quartz substrates.

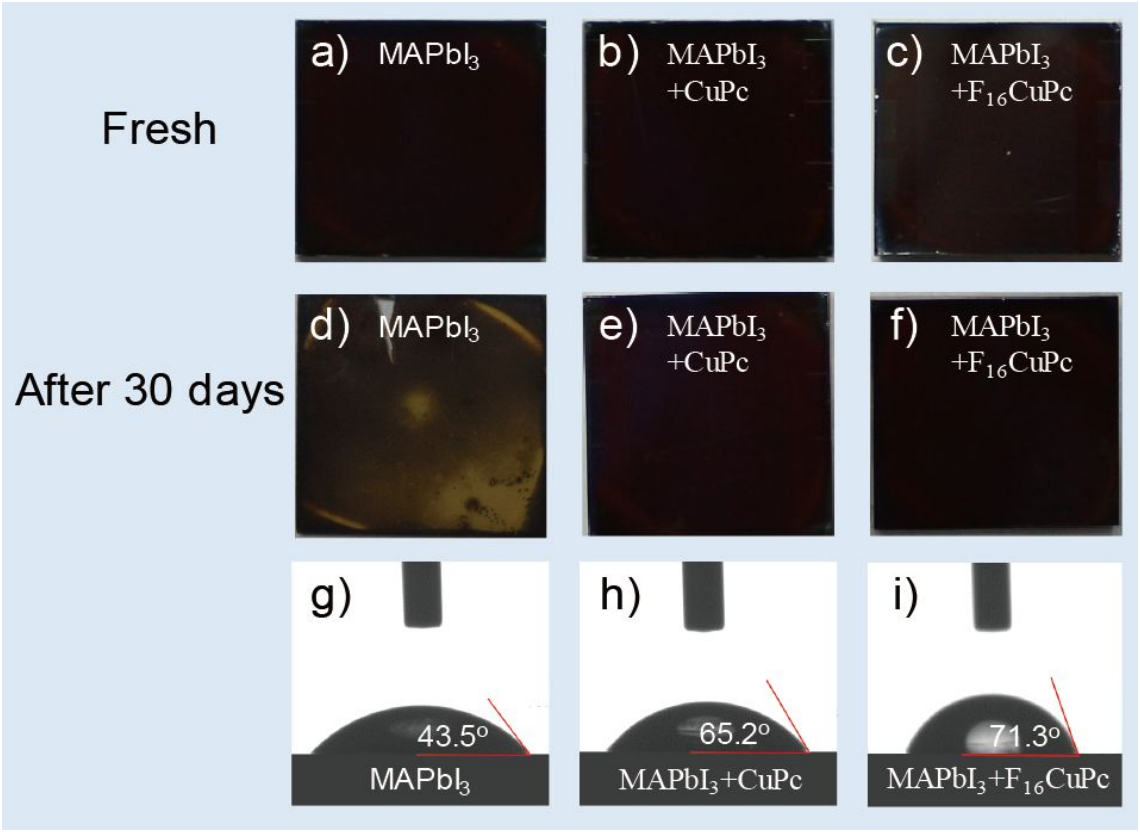

Figure S9. Images of a)-f) are the corresponding perovskite films before and after 30 days under the ambient environment with a 30% relative humidity at room temperature; the contact angles between perovskite films and the water droplet: g) $MAPbI_3$, h) $MAPbI_3$+CuPc, i) $MAPbI_3$+F_{16}CuPc.

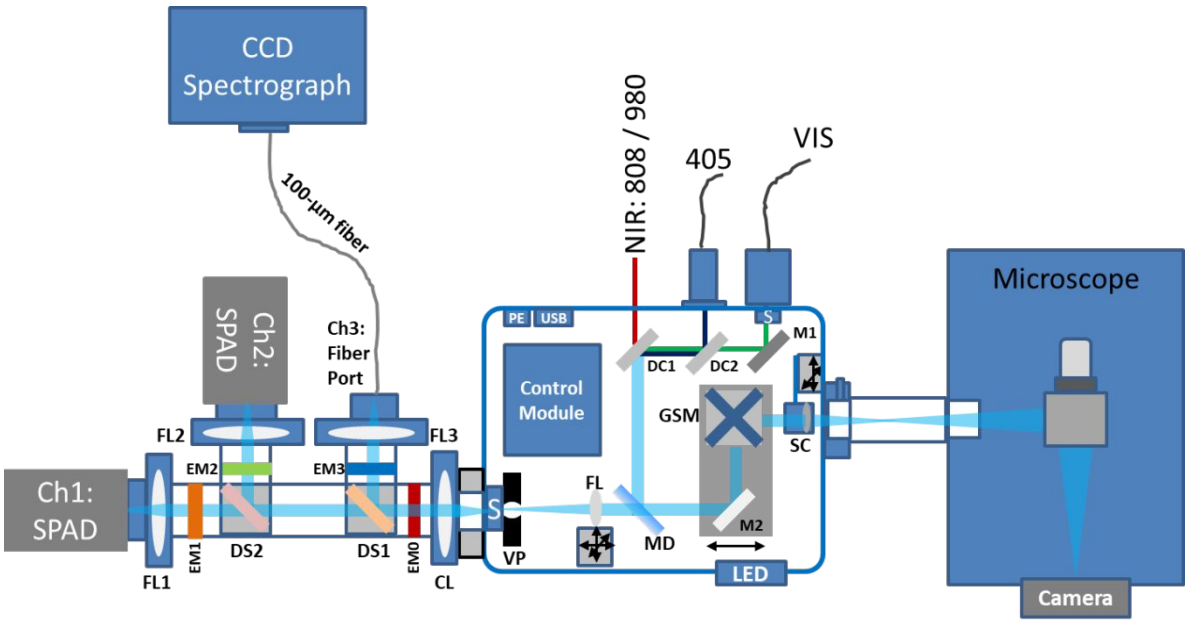

Figure S10. Schematic of the time-resolved confocal imaging system.

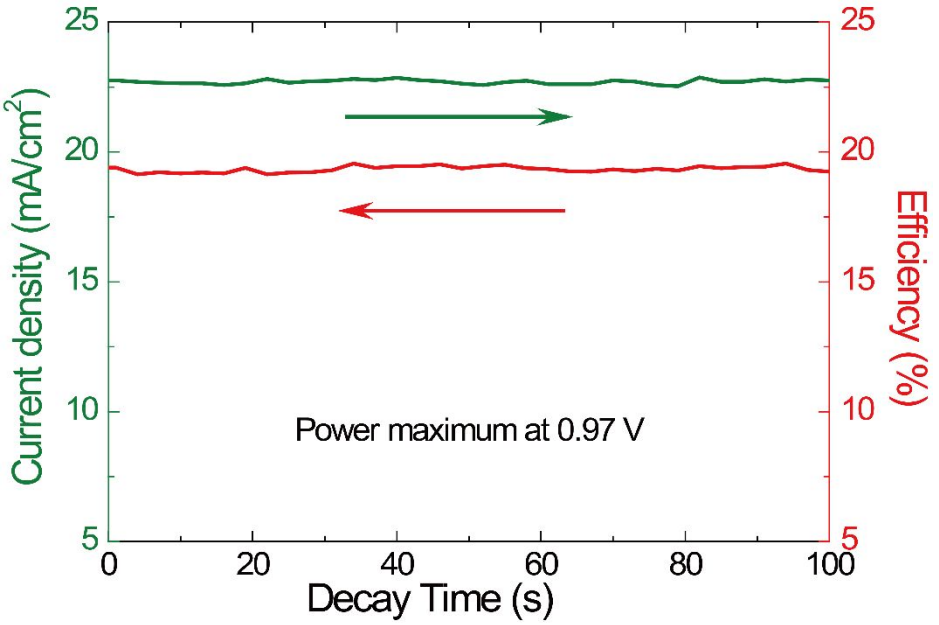

Figure S11 Steady output of photocurrent density and power conversion efficiency measured under maximum power at 0.97 V. The cell was illuminated under 1 sun AM1.5G prior to the start of the measurement.

Table S1 Photovoltaic parameters of planar heterojunction PSCs with different concentration of CuPc in CB.

CuPc in CB	V_{oc} (V)	J_{sc} (mA/cm^2)	*FF*	*PCE* (%)

0 mg/mL	1.07	22.7	0.77	18.7
0.1 mg/mL	1.10	22.6	0.77	19.1
0.2 mg/mL	1.11	22.7	0.78	19.7
0.3 mg/mL	1.10	22.3	0.77	18.9
0.4 mg/mL	1.07	22.3	0.75	17.9
0.5 mg/mL	1.08	21.7	0.76	17.8
0.6 mg/mL	1.06	21.5	0.73	16.6

Table S2 Photovoltaic parameters of planar heterojunction PSCs with different concentration of $F_{16}CuPc$ in CB.

$F_{16}CuPc$ in CB	V_{oc} (V)	J_{sc} (mA/cm^2)	FF	PCE [a)] (%)
0 mg/mL	1.07	23.0	0.77	18.9
0.1 mg/mL	1.11	22.9	0.77	19.3
0.2 mg/mL	1.15	22.9	0.78	20.2
0.3 mg/mL	1.13	22.8	0.76	19.6
0.4 mg/mL	1.14	22.9	0.75	19.4
0.5 mg/mL	1.08	23.1	0.76	18.9
0.6 mg/mL	1.09	22.4	0.74	17.9